Milankovitch Period Uncertainties and Their Impact on Cyclostratigraphy

David Waltham (d.waltham@rhul.ac.uk)

Department of Earth Sciences

Royal Holloway

University of London

Egham, Surrey TW20 0EX, UK

Abstract

Astronomically calibrated cyclostratigraphy relies on correct matching of observed sedimentary cycles to predicted astronomical drivers such as eccentricity, obliquity and climate-precession. However the periods of these astronomical cycles, in the past, are not perfectly known because: (i) they drift through time; (ii) they overlap; (iii) they are affected by the poorly constrained recession history of the Moon. This paper estimates the resulting uncertainties in ancient Milankovitch cycle periods and shows that they lead to: (i) problems with using Milankovitch cycles for accurate measurement of durations (potential errors are around 25% by the start of the Phanerozoic); (ii) problems with correctly identifying the Milankovitch cycles responsible for observed period ratios (e.g. the ratio for long-eccentricity/short-eccentricity overlaps, within error, with the ratio for short-eccentricity/precession); (iii) problems with verifying that observed cycles are Milankovitch driven at all (the probability of a random period-ratio matching a predicted Milankovitch-ratio, within error, is 20-70% in the Phanerozoic). Milankovitch-derived ages and durations should therefore be treated with caution unless supported by additional information such as radiometric constraints.

INTRODUCTION

Astronomically calibrated cyclostratigraphy (Hinnov, 2000; Weedon, 2003) has been used to refine the geological time-scale (e.g. Weedon et al., 1999; Gradstein et al., 2004; Peterson, 2011), estimate sedimentation rates (e.g. Meyers, 2008) and improve understanding of sedimentary processes in the past (e.g. Herbert, 1992). There are several approaches but they are generally equivalent to spotting multiple orders of cyclicity in the sedimentary record and matching their wavelength-ratios to the expected period-ratios of astronomical drivers. For example, “bundling” of packages of five cycles into larger repeated sequences may indicate the sedimentary effects of climate precession (with a period ~20ky) superimposed upon eccentricity (with a period ~100 ky) (Sander, 1936; Schwarzacher, 1947; Goldhammer et al., 1987; Gong et al., 2001). More sophisticated analyses utilize spectral techniques to identify the principal wavelengths in the data (Thomson, 1990; Williams; 1991; Paul et al., 2000; Tian et al., 2014) along with rigorous statistical techniques to reject statistically insignificant identifications and to evaluate uncertainty (e.g. Myers 2012; Hinnov, 2013; Zeeden et al., 2015). It is also possible to independently confirm longer cycles using radiometric dating (Hinnov and Hilgen, 2012; Boulila et al., 2014) and this greatly increases confidence in the analyses. Furthermore, “tuning” can considerably enhance results by forcing exact-regularity onto one of the observed cycles to compensate for fluctuations in sedimentation rate (e.g. Weedon et al. 1999; Huang et al., 2010).

However, Milankovitch cycle periods (and hence their ratios) are imperfectly known in the past and this may cause problems for cyclostratigraphy. In particular, any uncertainties in predicted periods give rise to corresponding uncertainties in estimates of observed time-durations and this, in turn, impacts on attempts to use cyclostratigraphy to refine the geological time-scale. Furthermore, sufficiently large uncertainties in period-ratios would make the hypothesis, that observed cycles are Milankovitch driven, difficult to test as any such contention will lack statistical significance (i.e. there is a high probability of hitting a plausible ratio by chance). It also becomes impossible to unambiguously assign cycles if the uncertainties are large enough to cause overlaps of adjacent ratios. Incorrect assignment of cycles would, in turn, undermine cyclostratigraphically estimated time-durations.

This paper makes first-order estimates of Milankovitch-period uncertainties so that the potential seriousness of these difficulties can be assessed. It does not discuss the considerable problems associated with analysing sediments to extract periodicities. Instead, it confines itself to issues that will arise even if the wavelengths of sedimentary cycles have been measured with zero error. In practice, data-derived wavelengths are far from perfect but such issues have been discussed by many authors (e.g. Hinnov, 2000 and 2013; Meyers 2013; Vaughan et al., 2012, 2014) and will not be discussed further here.

One source of uncertainty in predicted Milankovitch periods is that the cycles are not perfectly periodic but undergo “diffusive drift” as the mutual interactions between the planets chaotically perturb their orbits over tens of millions of years. For example, using Laskar et al.’s (2011) numerical modelling of the last 100 Ma, the “long eccentricity” variations can be approximated by a sinusoidal signal with a period of 405.6 ky but this period has a drift-generated variation of 2.4 ky. Table 1 shows the principal Milankovitch cycles investigated in this paper, along with their diffusive drift variation (after Laskar et al., 2011). Diffusive drift makes it impossible to extrapolate Earth’s detailed orbital parameters more than 40 Ma into the past (Laskar et al. 2004). In particular, the chaotic dynamics of the solar system makes it impossible to predict where we were, in a particular Milankovitch cycle, at distant times. For example, we can say that the ~124 ky eccentricity cycle almost certainly existed at 1 Ga but we cannot say where we were in the cycle, i.e. whether the eccentricity was small or large at that precise time. The current paper therefore estimates ancient Milankovitch periods but makes no attempt to estimate the amplitudes or phases of ancient Milankovitch cycles.

In addition to diffusive-drift, a further source of uncertainty is that several of the periods shown in Table 1 are sufficiently close to each other to make unique identification difficult. For example, two of the contributing periods to "short eccentricity" lie at 94.9±1.4 ky and 98.9±1.5 ky and so any identified spectral peak in sediments at around 95 ky could be produced by either of these cycles or by a combination of them both.

Uncertainties produced by diffusive drift and by overlap of nearby periods are included in this paper but most of the work reported here concerns another potential source of Milankovitch-period uncertainty; the poorly constrained recession history of our Moon (Webb, 1982; Williams, 1989; Berger et al. 1992; Berger and Loutre, 1994; Sonett et al., 1996; Bills and Ray, 1999; Williams, 2000; Mazumder and Arima; 2005). Friction, from tidally driven ocean currents, gradually slows the Earth's rotation and increases the Earth-Moon separation through time. The falling rotation rate reduces the size of Earth's equatorial bulge whilst lunar-recession produces a drop in tidal-forces and, together, these changes reduce the rate at which Earth's axis precesses. This precession rate is specified by the precession constant, k, which gives the change in orientation of the axis in seconds of arc per year ("/y) but which can be converted to a precession period = 1296/k thousand years.

Climate-precession cycles and obliquity cycles both result from interaction between axial-precession (which changes the orientation of Earth's axis) and orbital-precession (which changes the orientation of Earth's orbit). Climate precession is produced by the changing relationship between the timing of solstices (as Earth's axis precesses) and the timing of

Earth's closest approach to the Sun (as Earth's orbit precesses). Obliquity cycles, on the other hand, are produced by the changing difference between the orientation of Earth's axis and the orientation of its orbit. Hence, the periods of climate precession and obliquity both change through time as Earth-Moon system evolution produces a changing Earth-axis precession rate. The uncertain recession history of the Moon therefore leads to uncertainty in predicted climate-precession-cycle and obliquity-cycle periods.

To address this problem, ancient obliquity and climate-precession frequencies have previously been estimated by assuming that lunar-recession rate is constant (Berger et al., 1992); Berger and Loutre, 1994) or that the tidal-time-lag (a measure of tidal energy dissipation) is constant (Laskar et al., 2004). Unfortunately, neither assumption is valid. Constant recession at the present-day rate implies Moon formation at ~9.6 Ga whilst assuming that the present-day time-lag applies throughout Earth-history predicts Moon formation at ~1.5 Ga (Gerstenkorn, 1967). In contrast, age estimates for formation of the Earth-Moon system are around 4.5 Ga (e.g. Kleine et al., 2005; Taboul et al., 2007). The modern recession rate therefore overestimates the Earth-Moon separation in the past whilst the modern tidal-time-lag systematically underestimates it.

The underestimated time since Moon-formation, predicted by the constant tidal-time-lag model, implies that correct timing of Moon formation requires the typical tidal-time-lag, over Earth's history, to be substantially smaller than the observed value at the present day. The high, modern tidal-dissipation results from resonance effects in the Earth's oceans; some combinations of natural oscillation frequencies in ocean-basins are close to frequencies excited by the tides (Gotlib and Kagan, 1980, 1981; Platzman et al., 1981; Webb, 1982; Green 2010; Green and Huber, 2013). Hence relatively strong tidal currents are excited which produce increased tidal-friction at the sea-floor.

The strength of this resonance varied through time as a result of eustatic sea-level change, plate-tectonic reorganization of the basins and decreasing tidal-frequency as Earth's rotation slows. Hence, fluctuations in tidal-time-lag (resulting from eustacy and plate-tectonics) are superimposed upon a long-term trend (resulting from a gradually lengthening day). Some studies (e.g. Webb, 1982) imply that the resulting evolution is dominated by the long-term trend whilst others (e.g. Green and Huber, 2013) support the idea of large fluctuations. Settling this question by computer simulation of ancient tides is prevented by the computational-cost of the many, high-resolution models needed and by a lack of sufficiently well-constrained ancient ocean bathymetries. There has been some progress but only for the relatively recent past (e.g. Green and Huber (2013) model Eocene tides) and it is unlikely that sufficiently detailed bathymetries will soon be available for more distant periods of Earth history.

Given these difficulties, it is clearly desirable to find observational constraints on ancient Earth-Moon separation. In principle, these can be obtained using ancient tidal rhythmites; sediments that retain a record of the number of days per neap-spring tide-cycle and the number of neap-spring tide-cycles per year (Williams, 1989, 2000; Sonett et al., 1996a, 1996b; Bills and Ray, 1999; Mazumder and Arima, 2005). The Elatina and Reynella rhythmites of South Australia are the best published examples of tidal rhythmites since they record three independent measurements of Earth-Moon distance (Williams, 1989, 2000; Deubner, 1990). Together, these self-consistent determinations produce a combined separation estimate of 371±2 thousand km at 620±20 Ma.

However, as a consequence of errors resulting from missing laminations (Williams, 2000; Archer, 1996) and difficulties with correct recognition of cycles (Archer, 1996; Kvale et al., 1999), other rhythmites are not as well constrained as those from Elatina/Reynella and interpretations of all rhythmite deposits (including Elatina/Reynella) remain highly contentious. Alternate approaches have attempted to use banded iron formations (Walker and Zahnle, 1986) or stromatolites (Vanyo and Awramik, 1985; Cao, 1991) but none of these methods are widely accepted. Thus, there are no uncontentious measurements of Earth-Moon separation except for the present day value.

However, one other constraint is available. It is widely, but not universally, accepted that the Earth-Moon system formed as a consequence of a massive impact in the early solar system. This produced debris, orbiting the newly formed Earth, which coalesced to create the Moon just outside the Roche limit (Canup and Asphaug, 2001). Hence, an Earth-Moon separation of around 30 thousand km at 4.5 Ga is reasonably secure. In this paper, these two endpoints (i.e. 384 thousand km today and around 30 thousand km at 4.5 Ga) will be used to constrain reconstructions of Earth-Moon separation though time.

This leaves a great deal of uncertainty at other times and the effects of this, on Milankovitch cycle predictions, are the main focus of this paper. This paper does not provide significant, new advances in our understanding of the celestial mechanics of the Earth-Moon system. Neither does it provide new observational constraints. The paper's ambition is simply to take what we already know, and use this to make first-order estimates of uncertainties in cyclostratigraphic frequencies. The paper then looks at the consequences of those uncertainties for cyclostratigraphic interpretation of sediments. It must be emphasised that the uncertainties discussed here result from our ignorance concerning the details of Earth-

Moon system evolution and these uncertainties can in principle be removed by an improved understanding of that history (e.g. through better modelling of ancient tidal-drag or by obtaining better constraints from analysis of ancient sediments). However, such improvements lie outside the scope of this paper which is only concerned with quantifying the level and impact of current uncertainties.

In the next section a range of plausible Earth-Moon separation histories, consistent with the known end-points and celestial mechanics, will be investigated and used to place lower-limits on lunar recession uncertainties through time. Following this, these modelled lunar histories are used to calculate uncertainties in the Earth's axial precession rate. These uncertainties are then combined with those resulting from diffusive-drift and from overlapping-adjacent-periods, to produce estimates of uncertainties in Milankovitch periods and in their ratios. The paper concludes by discussing the resulting impacts on cyclostratigraphy and, in particular, on: (i) estimates of time-durations; (ii) identification of cycles; (iii) testing of the hypothesis that cycles are Milankovitch driven.

LUNAR RECESSION MODELLING

A Simplified Model

The first step is to investigate the Earth-Moon separation history. The theory of lunar recession was developed by Darwin (1880) and modern treatments can be found in Goldreich (1966), Murray and Dermott (1999), Atobe and Ida (2007) and Laskar et al. (2004). These papers provide detailed and comprehensive solutions to the problem of modelling Earth-Moon evolution but, throughout this paper, the simplifying assumptions of a zero-eccentricity, zero-inclination lunar-orbit will be made. These simplifications are necessary for the methods used here but the errors introduced are insignificant compared to those produced by lunar-recession uncertainty. If solar tides are also neglected (Deubner (1990) shows the effect is small) the evolution of the Earth-Moon separation becomes (Lambeck, 1980; Murray and Dermott, 1999; Bills and Ray, 1999)

$$\mathrm{d}a/\mathrm{d}t = f\, a^{-5.5}, \qquad (1)$$

where a is Earth-Moon separation, t is time and the tidal drag factor, f, is

$$f = 3\,(k_2/Q)\,(m/M)\,R^5\,\mu^{0.5}, \qquad (2)$$

with k_2 the Earth's Love-number (a measure of rigidity), Q the tidal quality factor (a measure of the rate of energy dissipation into heat), m and M the masses of the Moon and Earth respectively, R the radius of the Earth and $\mu = G(M + m)$. (Note that equations (1) and (2) can also be derived from the coplanar, zero-eccentricity, zero-solar-drag approximation to Laskar et al. (2004), equation (12) with Q^{-1} playing a role equivalent to their tidal-lag, Δt.) The stripped-down model given by equation (1) is used in preference to a numerical treatment of the full system of equations because it has the analytical solution

$$a^{6.5} = a_o^{6.5} - 6.5\, F_t\, t \qquad (3)$$

where a_o is the present day lunar distance, t is now age (i.e. there has been a change of sign from t representing time in equation (1)) and F_t is the age-averaged drag factor

$$F_t = \int_0^t f\, dt' \,/\, t\,. \qquad (4)$$

This simplified approach is surprisingly accurate as can be seen in Figure 1 which compares its predictions to Laskar et al.'s (2004) full solution. In Figure1, I have assumed a constant tidal drag of $F_t = 2.075 \times 10^{38}\ \mathrm{m}^{6.5}\ \mathrm{s}^{-1}$ (equivalent to Laskar et al.'s (2004) assumption of a constant time-lag of 639 s) which produces an rms difference between the models of only 0.015%.

Model Constraints

The tidal drag factor used in Figure 1 can be validated using lunar laser-ranging (Dickey et al., 1994) which gives a current recession rate of 38.2±0.7 mm/y and hence, from equation (1), $f = 1.99\pm0.04\text{x}10^{38}\ \text{m}^{6.5}\ \text{s}^{-1}$. This compares reasonably well to estimates from analysis of eclipse locations from 700 BC to 1990 AD (Stephenson and Morrison, 1995) which give a tidally generated reduction in day-length of 2.3±0.1 ms/century and, by conservation of angular momentum, a lunar-recession rate of 42.1±1.8 mm/y to yield f=2.2±0.1 x10^{38} $\text{m}^{6.5}\text{s}^{-1}$. Formal combination of these two estimates yields $f = 2.01\pm0.04\text{x}10^{38}\ \text{m}^{6.5}\ \text{s}^{-1}$ but the larger uncertainty in the eclipse-based estimate may reflect true, longer-term fluctuations not captured by the 40-year lunar-ranging datatset. The remainder of this paper will therefore be conservative by using a slightly larger estimate of uncertainty and assuming a present-day tidal-dissipation of $f = 2.1\pm0.1\text{x}10^{38}\ \text{m}^{6.5}\text{s}^{-1}$ which encompasses the best estimates from these two approaches and also ensures good agreement with the full model of Laskar et al. (2004). However, in the remainder of this paper, I assume that tidal dissipation varies through time so that F_t is no longer constant. Hence, $F_0 = 2.1\pm0.1\text{x}10^{38}\ \text{m}^{6.5}\text{s}^{-1}$ but, for all other times, F_t must be estimated.

The first stage is to find F_{4500}, i.e. the drag averaged over the entire history of the Earth-Moon system. Assuming the Moon formed as the result of a large impact at 4500±50 Ma (Touboul et al., 2007) just outside the Roche limit (i.e. a=3±1x10^7 m, Canup and Asphaug (2001)), equation (3) yields $F_{4500} = 6.85\pm0.08\ \text{x}10^{37}\ \text{m}^{6.5}\text{s}^{-1} = (0.33\pm0.03)F_0$. The mean tidal drag, averaged over the last 4.5 Gy, is therefore only one third of its present value.

This section will now model a range of plausible lunar-recession histories using equation (3) and the constraints that a_o=3.84x10^8m, F_o=2.1±0.1x10^{38} $\text{m}^{6.5}\text{s}^{-1}$ and $F_{4500} = 6.85\pm0.08\ \text{x}10^{37}$ $\text{m}^{6.5}\text{s}^{-1}$. These constraints, along with equation (3), ensure that a middle-path is taken for the predicted Earth-Moon separation which is neither biased towards too large a value (e.g. as produced by assuming the modern recession rate) nor too small a value (e.g. as produced by assuming a constant tidal-lag-time). Nevertheless, the constraints are not particularly restrictive and allow a wide range of possible scenarios.

To allow progress, this paper investigates two specific scenarios which are compatible with the constraints. First, I assume F_t increases smoothly through time as a consequence of a decelerating Earth-rotation rate. This produces a range of outcomes since the precise form of the smooth function is unknown. Following this, I look at a model in which f is assumed to slowly fluctuate around a long-term mean. This too produces a range of outcomes since there are many fluctuating sequences of f that have a long-term mean equal to F_{4500}.

Between them, these models predict a range of lunar-recession histories. If additional plausible models were also investigated, they could only serve to increase the range of predicted recession histories and so, provided the two models investigated here are plausible, they give a lower-bound estimate on the uncertainty. As will be shown, even this lower-bound is sufficient to demonstrate that astronomically-calibrated cyclostratigraphy is severely compromised.

Smooth Change Model

Ocean-tide models (Gotlib and Kagan, 1980, 1981; Platzman et al., 1981; Webb, 1982) based upon simplified ocean basin geometries (e.g. a constant-depth, hemispherical ocean in Webb (1982)) predict that tidal-drag increases, as Earth's rotation slows, until a resonance peak is reached at a slightly lower tidal-frequency than that experienced today. Thus, in these simplified models, f has increased through time and has not yet reached its maximum value. The broad effect of this form of f-history on predicted lunar distance can be demonstrated by using exponential growth to approximate this behaviour, i.e.

$$f = f_\infty + (f_0 - f_\infty)\exp(-t/\tau), \qquad (5)$$

where f_∞ is a background value and τ characterizes the timescale over which significant changes in resonance strength occur. This time-scale is poorly constrained, because of the simplifying assumptions of ocean-tide models, but since it is largely controlled by the time-scale for significant changes in Earth rotation rate, it should be on the order of 100s My or longer. Here, I will assume it falls in the range 100 My to 1 Gy.

Equation (3) requires the time-averaged drag F_t, rather than the instantaneous drag f, but integration of equation (5) gives

$$F_\mathrm{t} = f_\infty + (\tau / t)(f_0 - f_\infty)[1 - \exp(-t/\tau)]. \qquad (6)$$

The solid lines in Figure 2 show the resulting range of mean-tidal-drag histories with f_∞ chosen to ensure the correct value of F_{4500}. Figure 3 shows the resulting lunar-recession history. Both graphs only show the past 700 Ma because the Phanerozoic is the period of most interest in cyclostratigraphy whilst extending out to 700 Ma allows Figure 3 to compare models to the Earth-Moon distance derived from the Elatina/Reynella rhythmites.

Fluctuating Model

Time variation in f may have been dominated by eustatic sea-level changes or by plate-tectonic reorganization of ocean basins rather than by increasing day-length. Direct modelling of this is problematic, as already indicated, but the little modelling that has been done indicates that small changes in sea-level and basin geometry can produce dramatic changes in tidal dissipation (e.g. see Green and Huber, 2013). Hence, f may be better modelled as a complex fluctuation around a typical value. On this interpretation, the present-day high tidal-dissipation is a chance outlier.

The requirement for positive f, together with a modern value which exceeds the long-term mean by a factor of three, is inconsistent with the assumption that the fluctuations are normally-distributed around the mean but fully consistent with a log-normally distributed process. This subsection therefore builds a tidal-drag model based upon the assumption that drag fluctuated with a log-normal distribution having the correct long-term mean-drag and having fluctuations large enough to allow the high present-day value.

The mean, M, of a log-normal distribution is (DeGroot and Schervish, 2002)

$$M = \exp(m + \sigma^2/2) \quad (7)$$

where m is the location parameter and σ the scale parameter of the distribution. Furthermore, the cumulative probability is (DeGroot and Schervish, 2002)

$$P(x<X) = \Phi[\{ \ln(X) - m \} / \sigma], \quad (8)$$

where Φ is the cumulative distribution function of the normal distribution.

Combining equations (7) and (8), the probability of a randomly chosen value being at least three times the mean value is

$$P(x>3M) = 1.0 - \Phi[\ \ln(3)/\sigma + \sigma/2\ ]. \qquad (9)$$

Equation (9) is plotted in Figure 4 as a function of σ and shows that it is plausible for an outlier to exceed the mean by a factor of three (i.e. it has a probability >5%) but only for a narrow range of scale parameter. Hence, a log-normal-fluctuation explanation for the observed, large, modern *f* is statistically plausible (at 5% significance) and the remainder of this section approximates the Earth's tidal-drag history by a time-series of *f*-values extracted from a log-normal process.

The *f*-values in this time-series should be spaced sufficiently far apart that they are uncorrelated, independent specimens from the distribution. The appropriate time-interval depends upon the speed of the process causing changes in resonance strength. The longest relevant time-scale is that for significant reconfiguration of ocean basins whilst the shortest time-scale is associated with eustatic sealevel fluctuations. This unknown time-scale is the main source of uncertainty for the fluctuating-drag model but, in this paper, I will assume values in the range 0 to 100 My.

Over a period significantly greater than the time-scale, the mean value of *f* should converge onto the long-term mean. However, this simple situation is altered because the present-day value is known, rather than extracted from the distribution. As a result, the observed long-term mean is skewed away from the true mean and towards a higher value according to

$$F_{4500} = (\ nM + f_0\ )\ /\ (\ n + 1\ ) \qquad (10)$$

where *n* is the sample size, i.e.

$$n = 4500 / \Delta t \quad (11)$$

and Δt is the time-scale of the process (i.e. the gap between uncorrelated f values). Equation (10) allows the true-mean, M, of the distribution to be estimated from the observed long-term mean, F_{4500}. To completely specify the log-normal distribution a scale factor is also needed and I assume σ=1.48 since this gives the distribution for which the modern high-drag is least unlikely.

Given M and σ, the envelope of reasonable F_t functions can be found by noting that, for normal distributions, the sample mean fluctuates with a standard error equal to standard-deviation/√n (where n is sample size). Thus, for a log-normal distribution, the sample mean fluctuates around the population mean, M, with an asymmetric spread given by $M\exp(\pm\sigma/\sqrt{n})$ (i.e. ~68% of the sample means will lie in the range $M\exp(-\sigma/\sqrt{n})$ to $M\exp(+\sigma/\sqrt{n})$). Adding the constraint that f_0 is known then gives

$$F_{k\Delta t} = [\, f_0 + kM\exp(\pm\sigma/\sqrt{k}) \,] \,/\, (\, k + 1 \,) \quad (12)$$

as the envelope of time-averaged drags, F_t, at time $t=k\Delta t$.

The dashed lines in Figure 2 show the resulting envelope of F-histories assuming $0 < \Delta t <$ 100 My. The lower limit corresponds to control by eustatic sea level (fluctuations can occur on time scales << 1 My) whilst the upper limit corresponds to the time-scale for significant reorganization of ocean basins. This fluctuating-drag model produces generally lower predictions for F than the smooth-change model because the values fall towards the long-term mean more quickly as we go back in time. This is expected given that the assumed time-scale for the fluctuating model was 0-100 My whilst the assumed time-scale for the smooth-change model was 100-1000 My.

Comparison of Models and Data

The Earth-Moon separations produced by this paper's models are shown in Figure 3 along with the results from analysis of the tidal-rhythmites at Elatina/Reynella discussed in the introduction. The results of modelling lunar-recession assuming a constant tidal drag factor (i.e. the model of Laskar et al. (2004)) are also shown for comparison. The key observations are that the models introduced in this paper show significantly greater Earth-Moon separation than the constant-drag-factor model and much better agreement with the rhythmite data. Furthermore, the generally smaller drag-values of the fluctuating-drag model, compared to the smooth-change model, results in generally higher Earth-Moon separations at any given moment in time. This is the consequence of the smaller time-scale in the fluctuating model, as discussed above.

EARTH'S AXIAL PRECESSION FREQUENCY

The next step is to calculate Earth's precession frequency from the Earth-Moon separations found above. Following the methods described in Berger et al. (1992) but, as before, assuming a circular lunar-orbit, the axial precession frequency, k, is

$$k = A \cos(o)\, \Omega\, [\, (m/a^3) + (m_\odot/a_\odot^{\,3})\,] \qquad (13)$$

where A is a constant (chosen to make present day k=50.476 "/y, after Laskar et al. (2004)), o is obliquity, Ω is Earth's rotation frequency and $\odot$ indicates solar values. Earth's rotation rate and the obliquity can be calculated using the approach of Goldreich (1966) and Atobe and Ida (2007) which, under this paper's standard assumptions of circular, coplanar orbits and small solar effects, simplify to the equations

$$dx/da = -h(1 - x^2)(\Omega x - 2n) / 4aCx\Omega(\Omega x - n) \quad (14)$$

$$Cx\Omega = L_o - h \quad (15)$$

where C is Earth's moment of inertia, x=cos(o), h is the angular momentum of the lunar orbit (=$m'\mu^{1/2}a^{1/2}$), n is the lunar mean motion (=$\mu^{1/2}a^{-3/2}$), L_o is the conserved total angular momentum perpendicular to the lunar orbit, m' is the reduced lunar mass (=$mM/(m+M)$) and μ=G($m+M$). Explicit finite-difference solution of these equations (Press et al., 2002) gives Figure 5 which is indistinguishable from the full solution shown graphically in Goldreich (1966).

Using equations (13), (14) and (15), together with the previously derived results for lunar-recession, then produces the Earth-axis precession history shown in Figure 6. The key observation, from the point of view of this paper, is that the uncertainty in k increases with age and reaches around 10 "/yr by the early Phanerozoic.

THE IMPACT ON CYCLOSTRATIGRAPHY

Figure 7 shows the obliquity and climate-precession periods, along with their uncertainties, that result from combining Table 1 with Figure 6. Note that two of the climate-precession cycles given in Table 1 (P3 and P4) are indistinguishable on this plot and, hence, there are only four distinct cycles shown. The main conclusion is that the uncertainty in all the cycles increases rapidly with age, as a consequence of the uncertainty in Earth-Moon separation. Furthermore, by 150 Ma the uncertainties make two of the climate-precession cycles indistinguishable and, by 500 Ma, all of the climate-precession cycles have merged.

For obliquity, uncertainty rises from 0% today to 25% at the beginning of the Phanerozoic (~8 ky from the bottom of the range to the top, centred ~32 ky). As a consequence, any sedimentation durations calculated using obliquity cycles will also have errors of the same relative size and these could undermine attempts to use cyclostratigraphy to refine the geological time-scale.

Similar sized relative-errors also occur for the climate-precession cycles but, in this case, the situation is made more complex by the existence of four separate cycles. Two of the cycles (P3 and P4) are indistinguishable at all times and another two (P1 and P2) become indistinguishable before 150 Ma. All four cycles are indistinguishable before 500 Ma. By the start of the Phanerozic the uncertainty exceeds 35% (~7ky range centred ~19ky).

However, as discussed in the introduction, the true observables determined from analysis of sedimentary cycles are not usually cycle periods but, rather, ratios of sedimentary wavelengths. Figure 8 uses the periods (and associated uncertainties) from Figure 7 to calculate Milankovitch period ratios (and their uncertainties). Note that the 10 cycles listed in Table 1 give rise to 45 ratios but, for clarity, Figure 8 does not display them all. Firstly, related ratios which overlap have been collected together (e.g. the top of Figure 8 shows the 4 long-eccentricity/precession ratios as a single zone). Secondly, the 4 ratios of long-eccentricity/short-eccentricity are not plotted as they do not change with time (after including overlaps, these ratios are 4.19±0.17 and 3.19±0.17).

The first conclusion that can be drawn from Figure 8 is that some period-pairs are non-unique. Before 400 Ma, an observed period ratio of ~4.5 could result from short-eccentricity/precession or short-eccentricity/obliquity. Even more seriously, one of the long-eccentricity/short-eccentricity ratios (4.19±0.17) always overlaps with short-eccentricity/precession whilst the other long-eccentricity/short-eccentricity ratio (3.19±0.17) always overlaps with short-eccentricity/obliquity. As a consequence, there is potential to misidentify cycles. For example, an observed ratio of 4.2 might indicate that the shorter cycle is ~20 ky if it's precession-related or ~100 ky if it's short-eccentricity related. This would produce a five-fold difference in estimated time-duration.

A further problem indicated by Figure 8 is that, even at 0 Ma, there is a 20% probability that a randomly chosen ratio will fall within a predicted ratio-range. By the time we get to the start of the Phanerozoic there is a 70% chance of a randomly chosen ratio hitting a predicted Milankovitch-ratio uncertainty range. Under these circumstances, we cannot claim that finding a predicted ratio, in a sedimentary dataset, is a reliable indication that the cycles really are Milankovitch driven. Ideally, for identification of Milankovitch-cyclicity to be statistically significant, the probability of hitting a predicted ratio by chance should be below 5% (taking the standard assumption in Earth Sciences of a 5% significance level). Clearly, from Figure 8, this threshold is never met for a single observed ratio.

However, in most analyses of sedimentary data, several superimposed cycles will be observed allowing more than one wavelength-ratio to be estimated. If n independent wavelength ratios are found in the data, the probability of this occurring by chance is p^n where p is the probability of hitting a single ratio by chance. The number of independent ratios is, in turn, given by the number of cycles minus one (e.g. 3 cycles give only 2 independent ratios because the third ratio is simply related to the other two). Figure 9 shows the number of observed cycles required to bring the joint probability below 5%. For example, at 200 Ma, five different Milankovitch cycles should be identified to make the assumption of Milankovitch cyclicity statistically significant. Given this issue, it is important that additional constraints (e.g. radiometric dates) are available when claims are made of the identification of Milankovitch-driven cycles in sedimentary sequences.

CONCLUSIONS

This paper has, for the first time, made estimates of the uncertainties in Milankovitch cycle periods and their ratios. It has also investigated the impacts of these uncertainties on astronomically-calibrated cyclostratigraphy. The key conclusions are:

1. Obliquity-cycle and precession-cycle period uncertainties grow with time and are typically 10s of percent within the Phanerozoic. These uncertainties will produce similar sized uncertainties in sedimentation-duration estimates made using cyclostratigraphy.
2. These uncertainties in Milankovitch periods are large enough to produce substantial overlaps between adjacent periods. As a consequence, there is frequently ambiguity concerning correct identification of cycles and, hence, serious problems with estimation of sedimentation durations.
3. Cyclostratigraphy often relies on identification of ratios of Milankovitch cycle pairs (e.g. 5:1 bundling of eccentricity to precession) rather than direct identification of individual cycles. However, these ratios have substantial uncertainties and the resulting overlaps produce severe non-uniqueness in the identification of cycles. These will translate into substantial uncertainties concerning estimation of durations.

4. Once uncertainties are taken into account, the predicted ratios of Milankovitch cycles cover a large percentage of the available space. Hence, finding a wavelength-ratio in sedimentary cycles which matches predicted Milankovitch-ratios is not statistically significant. Several ratios must therefore be identified before Milankovitch cyclicity can be confidently established and this difficulty gets worse the further back in time we go. Hence, in the absence of independent methods for estimating durations (e.g. radio-active decay based methods), it is difficult to demonstrate that cycles are Milankovitch driven.
5. Previous estimates of lunar recession have systematically overestimated Earth-Moon separation in the past (if they assumed constant recession rate) or systematically underestimated Earth-Moon separation (if they assumed constant tidal time-lag). The estimates produced in this paper do not have either bias and, for the first time, include estimates of uncertainty. They should therefore be used in preference to earlier estimates until better observational constraints become available.
6. The uncertainties for obliquity and climate-precession periods are dominated by the effect of uncertainties in lunar-recession history. Hence, the effectiveness of cyclostratigraphy would be significantly enhanced if better estimates of past Earth-Moon separation could be produced.
7. The calculations used in this paper have been incorporated into a JavaScript program that can be run on any modern browser on any device (Fig 11). The program calculates Earth-Moon separation, day-length, axial precession period, the main obliquity period and the four main climate-precession periods for any time in Earth history. It also gives the corresponding uncertainties. The program is released under a creative commons licence and can be freely downloaded from

http://nm2.rhul.ac.uk/project/cyclostratigraphy-evolution-earth-moon-system/. Once downloaded, the program can be distributed without restriction.

Acknowledgements: Peter Burgess made invaluable suggestions, concerning the paper's emphasis, after reading an earlier version. The reviewers (Stephen Myers and Linda Hinnov) provided constructive and insightful comments that highlighted several weaknesses and also greatly improved the manuscript's clarity.

References

Archer, A.W., 1996, Reliability of lunar orbital periods extracted from ancient cyclic tidal rhythmites, Earth and Planetary Science Letters, v. 141, p. 1-10.

Atobe, K., and Ida, S., 2007, Obliquity evolution of extrasolar terrestrial planets. Icarus, v. 188, p. 1-17.

Berger, A., Loutre, M.F., and Laskar, J., 1992, Stability of the Astronomical Frequencies Over the Earth's History for Paleoclimate Studies, Science, v. 255, p. 560-566.

Berger, A., and Loutre, M.F., 1994, Astronomical forcing through geological time, *in* de Boer, P.L., and Smith, D.G., eds., Orbital Forcing and Cyclic Sequences, IAS special publication, v. 19, p. 15-24.

Bills, B.G., and Ray, R.D., 1999, Lunar Orbital Evolution: A Synthesis of Recent Results, Geophysical Research Letters, v. 26, p. 3045-3048.

Boulila, S., Galbrun, B., Huret, E., Hinnov, L.A., Rouget, I., Gardin, S., Huang, C., and Bartolini, A., 2014, Astronomical calibration of the Toarcian Stage: implications for sequence stratigraphy and duration of the early Toarcian OAE, Earth and Planetary Science Letters, v. 386, p. 98-111.

Canup, R.M., and Asphaug, E., 2001, Origin of the Moon in a giant impact near the end of the Earth's formation, Nature, v. 412, p. 708-712.

Cao, R., 1991, Origin and order of cyclic growth patterns in matministromatolite bioherms from the Proterozoic Wumishan formation, North China. Precambrian Research, v. 51: p. 167-178.

Darwin, G.H., 1880, On the Secular Changes in the Elements of the Orbit of a Satellite Revolving about a Tidally Distorted Planet, Philosophical Transactions Royal Society London,. v. 171, p.713-891.

DeGroot, M.H., and Schervish, M.J., 2002, Probability and Statistics, Addison Wesley, Boston, 816p.

Deubner, F-L., 1990, Discussion on Late Precambrian tidal rhythmites in South Australia and the history of the Earth's rotation, Journal Geological Society, v. 147, p. 1083-1084.

Dickey, J.O., Bender, P.L., Faller, J.E., Newhall, X.X., Ricklefs, R.L., Ries, J.G., Shellus, P.J., Veillet, C., Whipple, A.L., Wiant, J.R., Williams, J.G., and Yoder C.F., 1994, Lunar laser ranging: A continuing legacy of the Apollo Program, Science, v. 265, p. 482-490.

Gerstenkorn, H., 1969, The earliest past of the Earth-Moon system. Icarus, v. 11, p. 189-207.

Goldhammer, R.K., Dunn, P.A., and Hardie, L.A., 1987, High-frequency Glacio-Eustatic Sealevel Oscillations with Milankovitch Characteristics Recorded in Midlle Triassic Platform Carbonates in Northern Italy, Americam Journal of Science, v. 287, p. 853-892.

Goldreich, P., 1966, History of the Lunar orbit, Reviews of Geophysics, v. 4, p. 411-439.

Gong, Y., Li, B., Wang, C., and Wu, Y., 2001, Orbital cyclostratigraphy of the Devonian Frasnian-Famennian transition in South China, Palaeogeography, Palaeoclimatology, Palaeoecology, v. 168, p. 237-248.

Gotlib, V.Yu., and Kagan, B.A., 1980, Resonance periods of the World Ocean, Doklady Akademii Nauk SSSR, v. 252, p. 725-728.

Gotlib, V.Yu., and Kagan, B.A., 1981, On the resonance excitation of semidiurnal tides in the World Ocean, Izvestia Akadamii Nauk SSSR Fizika Atmosferi I Okeana, v. 17, p. 502-512.

Gradstein, F., Ogg, J., and Smith, A., 2004, A geologic time-scale 2004: Cambridge, Cambridge University Press, 589 p.

Green, J.A.M., and Huber, M. 2013, Tidal dissipation in the early Eocene and implications for ocean mixing, Geophysical Research Letters, v. 40, doi:10.1002/grl.50510.

Herbert, T.D., 1992, Paleomagnetic calibration of Milankovitch cyclicity in Lower Cretaceous sediments, Earth and Planetary Science Letters, v. 112, p. 15-28.

Hinnov, L., 2000, New perspectives on orbitally forced stratigraphy, Annual Review Earth Planetary Science, v. 28, p. 419–75.

Hinnov, L.A., and Hilgen, F., 2012, Chapter 4: Cyclostratigraphy and Astrochronology, in Gradstein, F., Ogg, J., Ogg, G., Smith, D., eds., A Geologic Time Scale 2012, Elsevier, p. 63-83.

Hinnov, L.A., 2013, Cyclostratigraphy and its revolutionizing applications in the Earth and planetary sciences, GSA Bulletin, v. 125, p. 1703-1734, doi: 10.1130/B30934.1.

Huang, C., Hesselbo, S.P., and Hinnov, L.A., 2010, Astrochronology of the Late Jurassic Kimmeridge Clay (Dorset, England) and implications for Earth system processes, Earth Planetary Science Letters, v. 289, p. 242-255.

Kleine, T., Palme, H., Mezger, K., and Halliday, A.N., 2005, Hf-W Chronometry of Lunar Metals and the Age and Early Differentiation of the Moon, Science, v. 310, p. 1671-1674, DOI: 10.1126/science.1118842.

Kvale, E.P., Johnson, H.W., Sonett, C.P., Archer, A.W., and Zawistoki, A., 1999, Calculating lunar retreat rates using tidal rhythmites, Journal of Sedimentary Research, v. 69, p. 1154-1168.

Lambeck, K., 1980, The Earth’s Variable Rotation, CUP, Cambridge.

Laskar, J., 1999, The limits of Earth orbital calculations for geological time-scale use, Philosophical Transactions Royal Society London. A, v. 357, p. 1735-1759.

Laskar, J., Robutel, P., Joutel, F., Gastineau, M., Correia, A.C.M., and Levrard, B., 2004, A long-term numerical solution for the insolation quantities of the Earth, Astronomy and Astrophysics, v. 428, p. 261-285.

Laskar, J., Fienga, A., Gastineau, M., and Manche, H., 2011, La2010: a new orbital solution for the long-term motion of the Earth, Astronomy and Astrophysics, v. 532, DOI: 10.1051/0004-6361/201116836.

Mazumder, R and Arima, M., 2005, Tidal rhythmites and their implications, Earth Science Reviews, v. 69, 79-95.

Meyers, S.R., 2008, Resolving Milankovitch controversies: The Triassic Latemar Limestone and the Eocene Green River Formation, Geology, v. 36, p. 319-322, doi: 10.1130/G24423A.1.

Meyers, S.R., Sageman, B.B., and Pagani, M., 2008, Resolving Milankovitch: Consideration of signal and noise, American Journal of Science, v. 308, p. 770-786, doi: 10.2475/06.2008.02.

Meyers, S.R., 2012, Seeing red in cycle stratigraphy: Spectral noise estimation for astrochronology. Paleoceanography, v. 27, doi: 10.1029/2012PA002307.

Murray, C.D., and Dermott, S.F., 1999, Solar System Dynamics, Cambridge University Press, New York, 592 p.

Paul, H.A., Zachos, J.C., Flower, B.P., and Tripati, A., 2000, Orbitally induced climate and geochemical variability across the Oligocene/Miocene boundary, Palaeoceanography, v. 15, p. 471-486.

Peterson, J.A., 2011, Better mathematical constraints on ages of Carboniferous stage boundaries using radiometric tuff dates and cyclostratigraphy, Geochemistry, geophysics, geosystems, v. 12, doi:10.1029/2010GC003467.

Platzman, G.W., Curtis, G.A., Hansen, K.S., and Slater, R.D., 1981, Normal modes of the World Ocean. Part II. Description of modes in the period range 8 hours to 80 hours, Journal of Physical Oceanography, v. 1, p. 579-603.

Press, W.H., Teukolsky, S.A., Vetterling, W.T., and Flannery, B.P. 2002, Numerical Recipes in C++, Cambridge University Press, Cambridge.

Sander, B. 1936, Beiträge zur Kenntnis der Anlagerungsgefüge (Rhythmische Kalke und Dolomiten aus Tirol), Tschermaks Mineralogische und Petrographische Mitteilungen, v.46, p. 27-209.

Schwarzacher, W., 1947, Ueber die sedimentare Rhythmik des Dachsteinkalkes von Lofer, Geolische Bundesanstalt., Vien, 1947, 10-12, 175-188.

Sonett, C.P., Kvale, E.P., Zakharian, A., Chan, M.A., and Demko, T.M., 1996a, Later Proterozoic and Paleozoic Tides, Retreat of the Moon, and Rotation of the Earth, Science, v. 273, p. 100-104.

Sonett, C.P., Zakharian, A., and Kvale, E.P., 1996b, Ancient tides and length of day: correction, Science, v. 274, p. 1068-1069.

Stephenson, F.R., and Morrison, L.V., 1995, Long-term Fluctuations in the Earth's Rotation: 700 BC to AD 1990, Philosophical Transactions Royal Society A, v. 351, p. 165-202.

Thomson, D., J. 1990, Quadratic-Inverse Spectrum Estimates: Applications to Palaeoclimatology, Philosophcal Transactions: Physical Sciences and Engineering, v. 332(1627), p. 539-597.

Tian, S., Chen, Z., and Huang, C., 2014, Orbital Forcing and Sea-Level Changes in the Earliest Triassic of the Meishan Section, South China. Journal Earth Science, v. 25, p. 64-73.

Touboul, M., Kleine T., Bourdon, B., Palme, H., and Wieler, R., 2007, Late formation and prolonged differentiation of the Moon inferred from W isotopes in lunar metals, Nature, v. 450, p. 1206-1209.

Vanyo, J.P., and Awramik, S.M., 1985, Stromatalites and Earth-Sun-Moon Dynamics, Precambrian Research, v. 29, p. 121-142.

Vaughan, S., Bailey, R. J., and Smith, D. G., 2011. Detecting cycles in stratigraphic data: Spectral analysis in the presence of red noise, Paleoceanography, v. 26, PA4211, doi:10.1029/2011PA002195.

Vaughan, S., Bailey, R. J., and Smith, D. G., 2014. Cyclostratigraphy: data filtering as a source of spurious .spectral peaks. From: Smith, D. G., Bailey, R. J., Burgess, P.M., and Fraser, A. J. (eds) Strata and Time: Probing the Gaps in Our Understanding. Geological Society, London, Special Publications, v. 404, doi:10.1144/SP404.11

Walker, J.C.G., and Zahnle, K.J., 1986, Lunar nodal tide and distance to the Moon during the Precambrian, Nature, v. 320, p. 600-602.

Webb, D.J., 1982, Tides and the evolution of the Earth-Moon system, Geophysical Journal Royal Astronomical Society, v. 70, p. 261-271.

Weedon, G.P., Jenkyns H.C., Coe, A.L., and Hesselbo, S.P., 1999, Astronomical calibration of the Jurasic time-scale from cyclostratigraphy in British mudrock formations, Philosophical Transactions Royal Society London, v. A357, p. 1787-1813.

Weedon, G.P., 2003, Time-Series Analysis and Cyclostratigraphy, CUP, Cambridge.

Williams, G.E., 1989, Late Precambrian tidal rhythmites in South Australia and the history of the Earth's rotation, Journal Geological Society, v. 146, p. 97-111.

Williams, G.E., 1991, Milankovitch-band cyclicity in bedded halite deposits contemporaneous with Late Ordovician-Early Silurian glaciation, Canning Basin, Western Australia, Earth and Planetary Science Letters, v. 103, p. 143-155.

Williams, G.E., 2000, Geological constraints in the precambrian history of Earth's rotation and the Moon's orbit, Reviews of Geophysics, v. 38, p. 37-59.

Zeeden, C, Myers, S.R., Lourens, L.J., and Hilgen, F.J., 2015, Testing astronomically tuned age models. Paleoceanography, v. 30, doi: 10.1002/2014PA002762.

Figure Captions

Figure 1. Comparison of equation (3) to the full numerical solution of Laskar et al. (2004). The rms difference is 0.015%.

Figure 2. Time-averaged tidal-drag factor, *F*, through time. Solid lines show the plausible range assuming tidal drag has risen smoothly through time. Dashed lines show the plausible range assuming the drag factor has fluctuated through time.

Figure 3. Lunar-recession history. Solid lines and dashed lines correspond to equivalent lines from Figure 2. The single point, with error bars, shows results from analysing the Elatina/Reynella rhythmites. The dotted line shows the constant-drag model (i.e. the model of Laskar et al. (2004)).

Figure 4. Probability of the modern tidal-drag exceeding three-times the long-term mean, as a function of log-normal scale parameter, σ. This probability exceeds 5% for a (narrow) range of σ and it is therefore plausible that the modern high value represents an outlier from a log-normal distribution.

Figure 5. Obliquity of Earth's axis as a function of Earth-Moon separation. Calculations assumed a circular lunar orbit and neglected solar effects. Separation is expressed in Earth-radii to allow easy comparison to the full solution of Goldreich (1966).

Figure 6. Earth's axial precession rate history. Solid lines and dashed lines correspond to those shown in figs. 2 and 3.

Figure 7. Climate-precession and obliquity periods, together with uncertainties, as a function of age. Two of the precesion periods (P3 and P4 from Table 1) are combined into a

single range as they are very close to one-another. Note that, by the start of the Phanerozoic, the period uncertainty (i.e. the range) is ~25% of the central estimate for both obliquity and precession.

Figure 8. Ratios of Milankovitch cycles as a function of time. Note that the cycles listed in Table 1 give rise to 45 separate ratios but, since uncertainties produce overlaps in many of these, the ratios are represented by the 5 zones shown here plus two zones for the ratios of long eccentricity to short eccentricity (4.19±0.17 and 3.19±0.17, not shown).

Figure 9. Probability that a randomly chosen ratio will agree, by chance, with a predicted Milankovitch cycle ratio within error. Note that, even at 0 Ma, a single observed ratio is insufficient to give a statistically significant identification (i.e. p>5%).

Figure 10. Number of observed cycles required for a statistically significant attribution to Milankovitch cyclicity. If the number of observed cycles is below this threshold, additional constraints are required (e.g. radiometric dating) to support a claim of Milankovitch cyclicity.

Figure 11. JavaScript Program for calculating ancient Milankovitch periods, and their uncertainties, using the methods described in this paper. The program is available at http://nm2.rhul.ac.uk/project/cyclostratigraphy-evolution-earth-moon-system/ and can be downloaded and redistributed freely.

Table 1. The major Milankovitch cycles, focussed on in this paper, along with their variability resulting from diffusive drift. The present day axial precession rate, k, is taken to be 50.476 "/y. Values in Table 1 are taken from Laskar et al (2011). Letters after precession cycles (P1, P2 etc) refer to abbreviations used in Fig. 7.

Cycle	**Freq ("/y)**	**Present Day Period (ky)**
Long Eccentricity	3.196 ± 0.019	405.6 ± 2.4
Short Eccentricity	13.66 ± 0.20	94.9 ± 1.4
Short Eccentricity	10.46 ± 0.20	123.9 ± 2.6
Short Eccentricity	13.11 ± 0.20	98.9 ± 1.5
Short Eccentricity	9.92 ± 0.20	130.8 ± 2.9
Obliquity	k - 18.848 ± 0.066 ± Δk	40.977 ± 0.086
Climate Precession, P1	k + 4.257482 ± 0.00003 ± Δk	23.678377 ± 0.000013
Climate Precession, P2	k + 7.453 ± 0.019 ± Δk	22.3722 ± 0.0074
Climate Precession, P3	k+ 17.92 ± 0.20 ± Δk	18.950 ± 0.055
Climate Precession, P4	k + 17.37 ± 0.20 ± Δk	19.103 ± 0.056

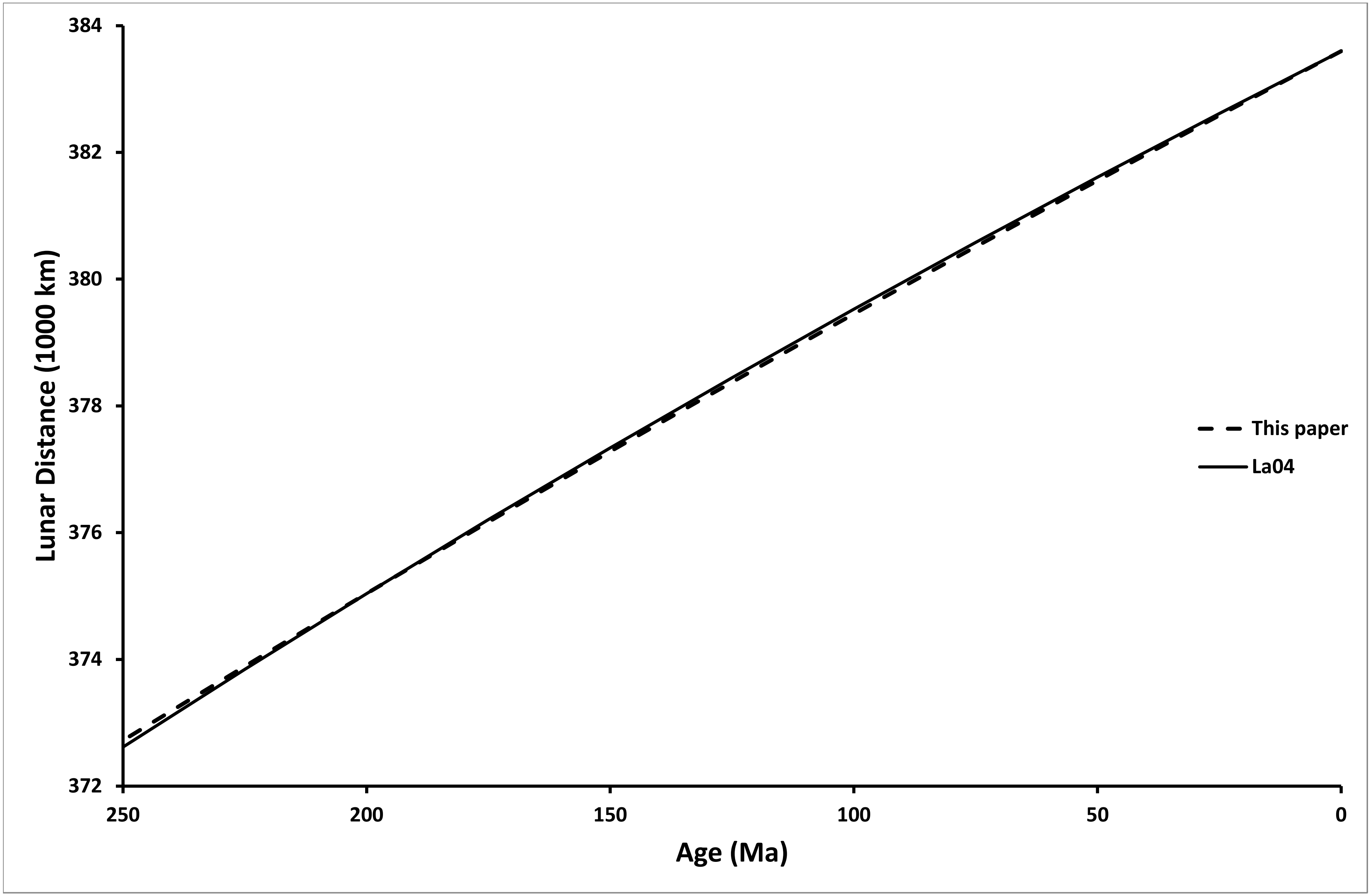

384
382
380
378
376
374
372
Lunar Distance (1000 km)
250
200
150
100
50
0
Age (Ma)
This paper
La04

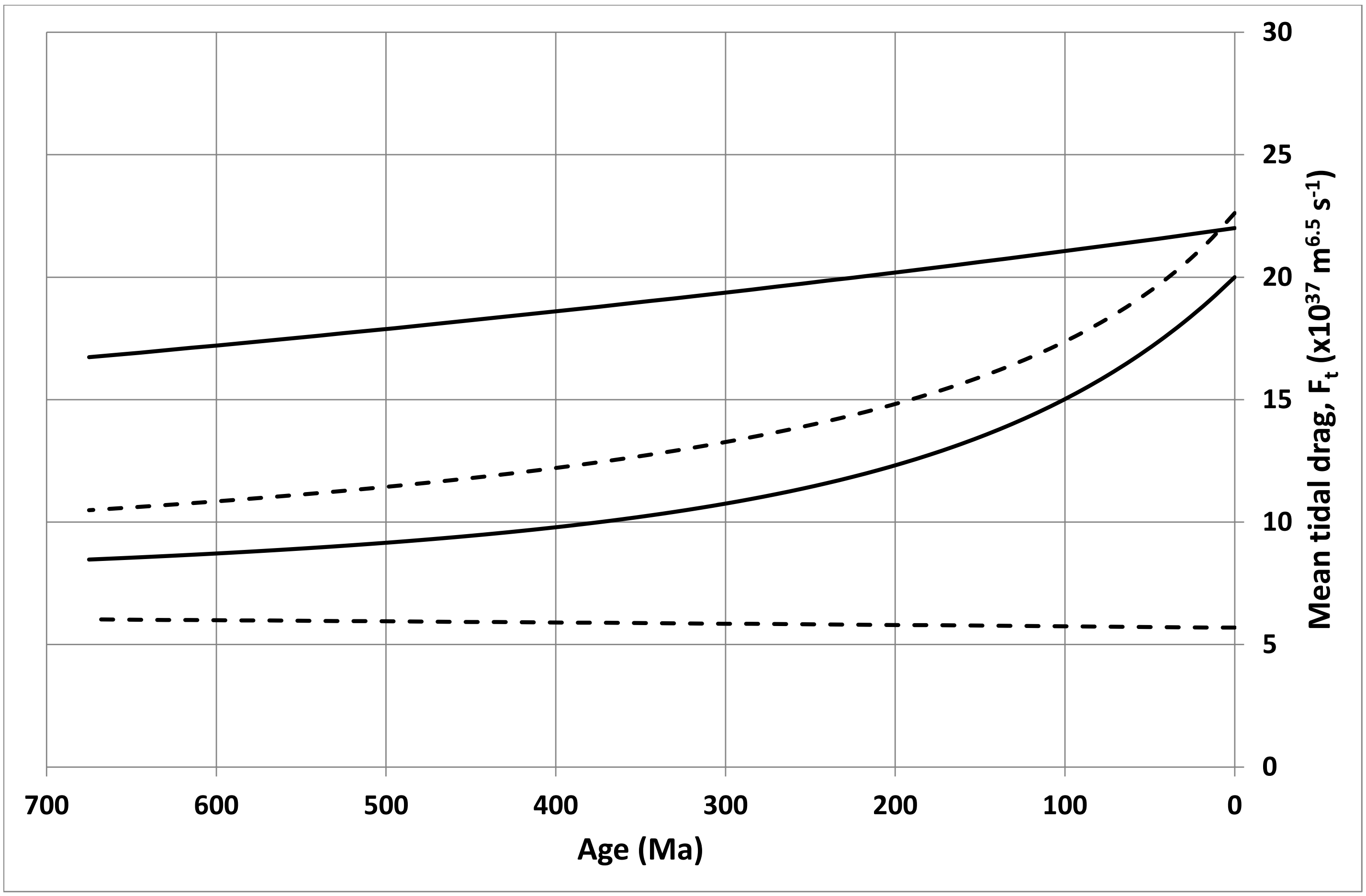

30
25
20
15
10
5
0
700
600
500
400
300
200
100
0
Age (Ma)
Mean tidal drag, F_t (x10^{37} m$^{6.5}$ s^{-1})

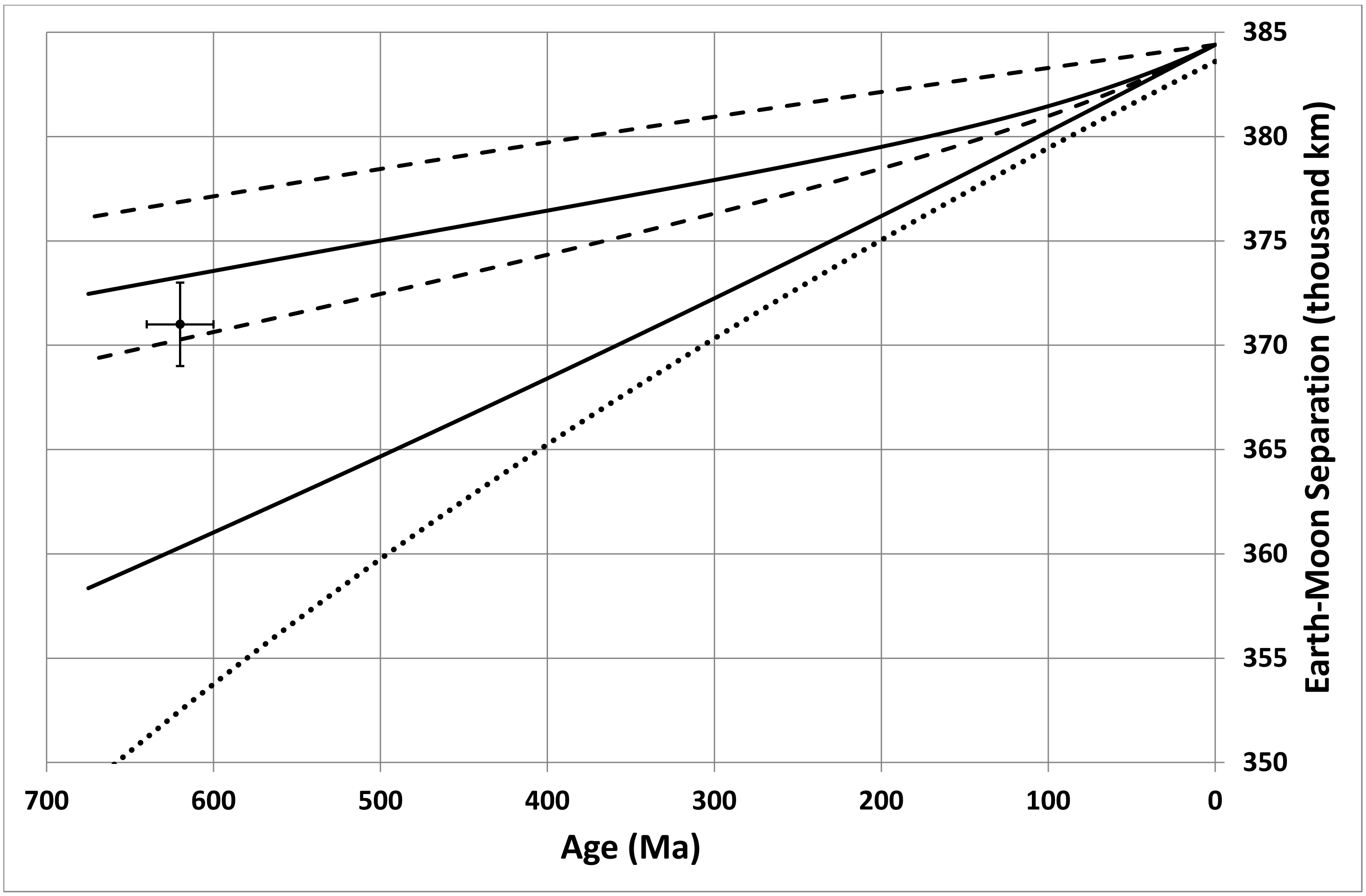

385
380
375
370
365
360
355
350
700
600
500
400
300
200
100
0
Age (Ma)
Earth-Moon Separation (thousand km)

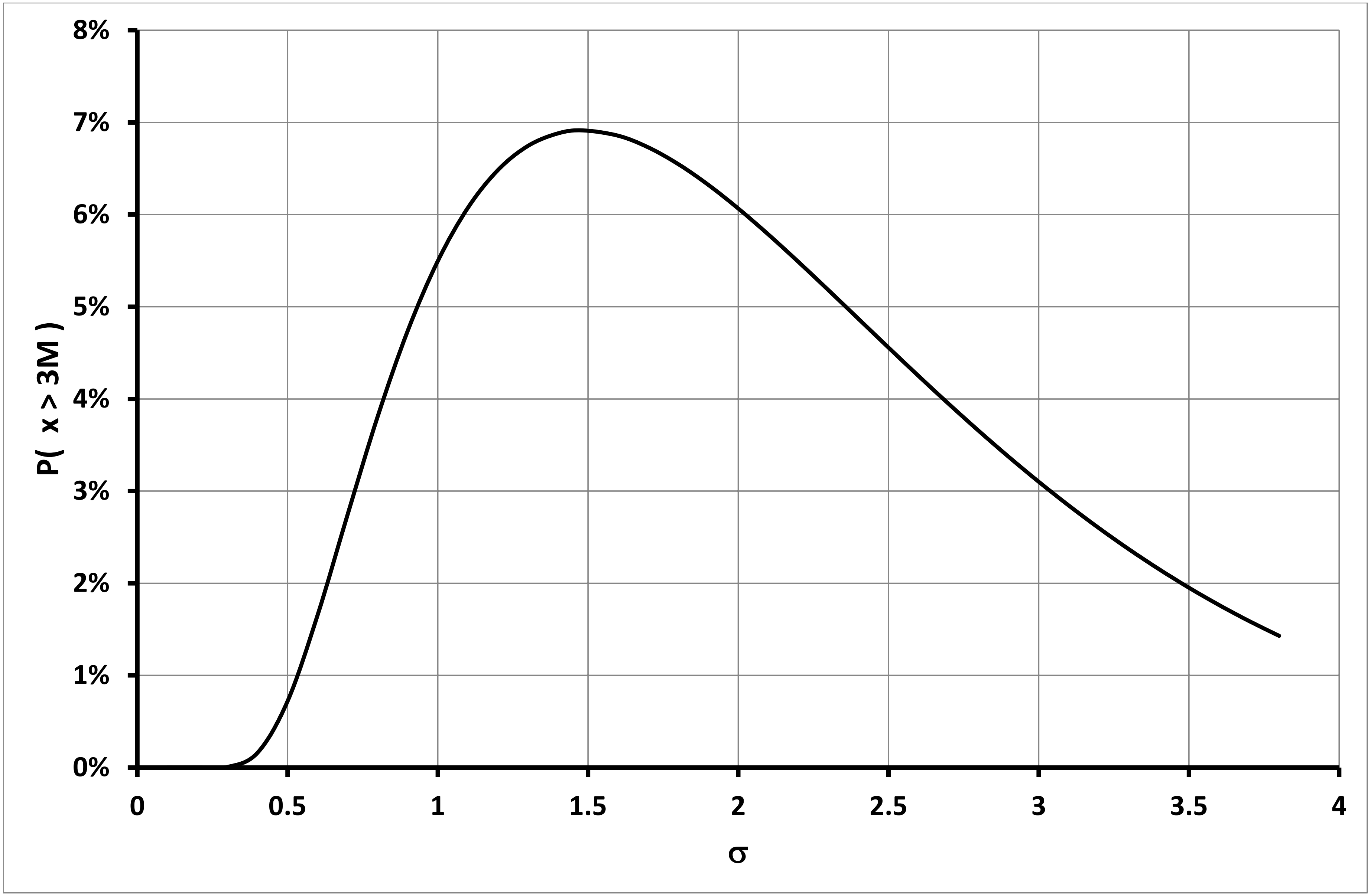
8%
7%
6%
5%
4%
3%
2%
1%
0%
P(x > 3M)
0
0.5
1
1.5
2
2.5
3
3.5
4
σ

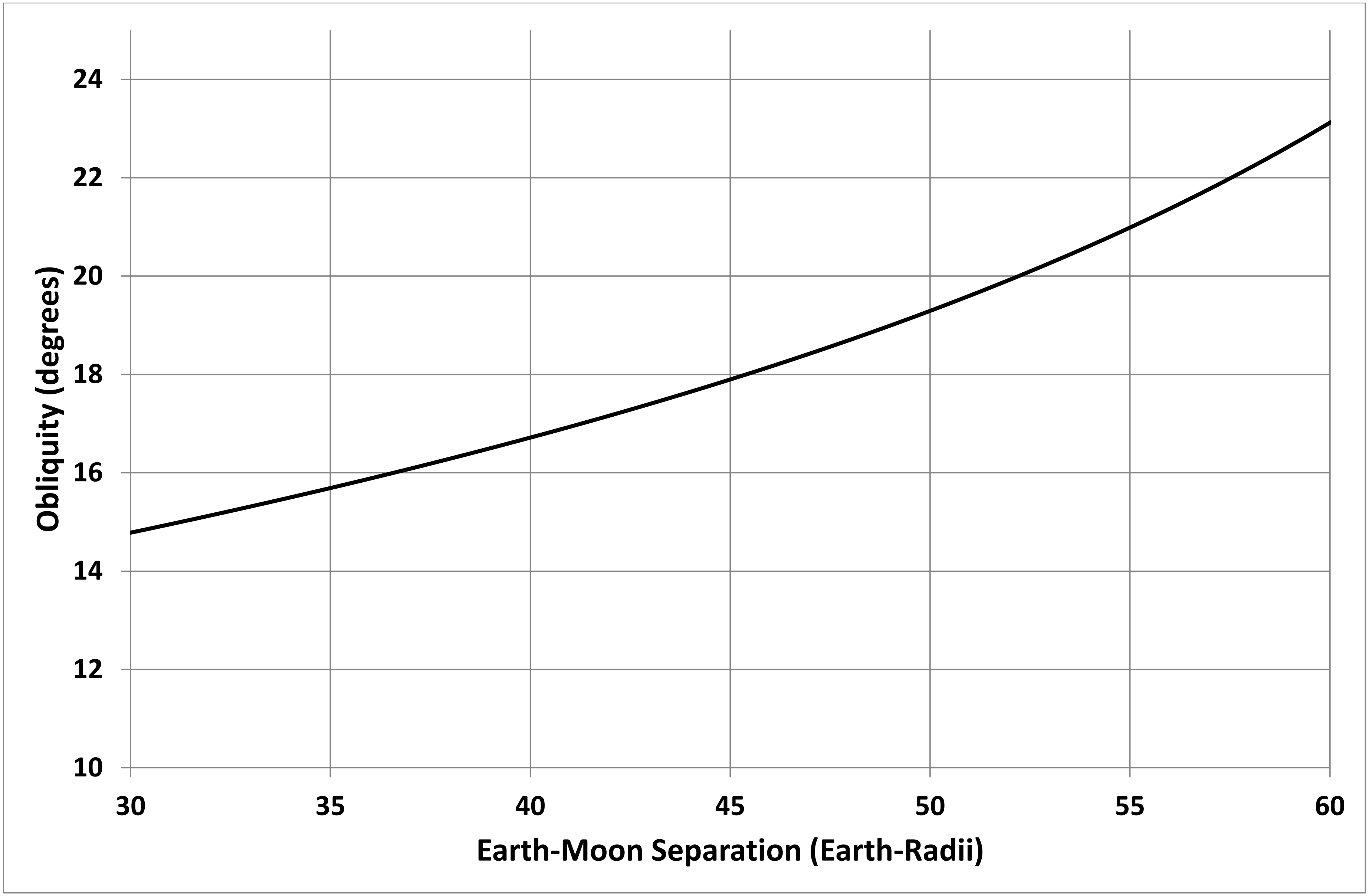
24
22
20
18
16
14
12
10
Obliquity (degrees)
30
35
40
45
50
55
60
Earth-Moon Separation (Earth-Radii)

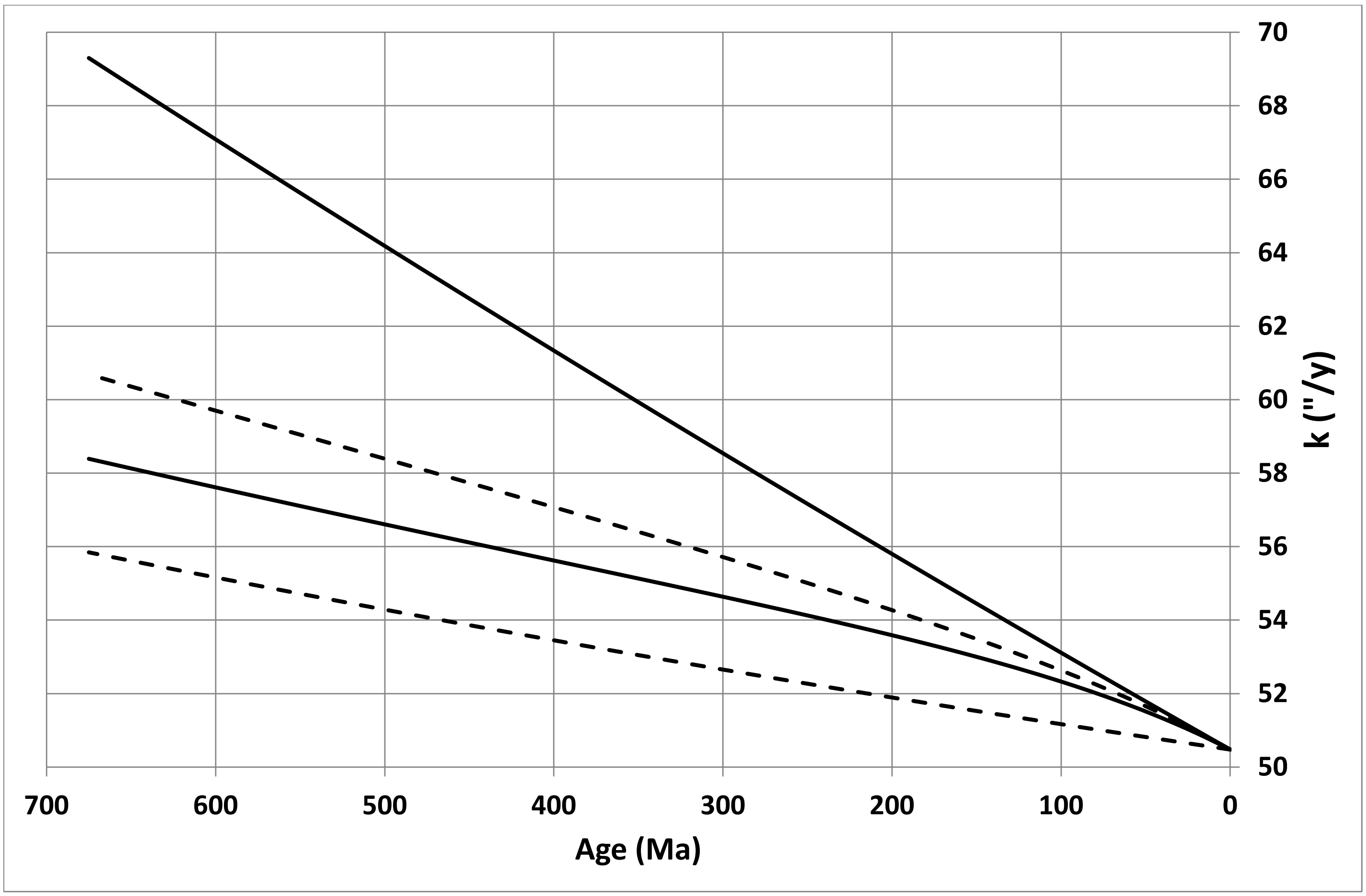

70
68
66
64
62
60
58
56
54
52
50
k ("/y)
700
600
500
400
300
200
100
0
Age (Ma)

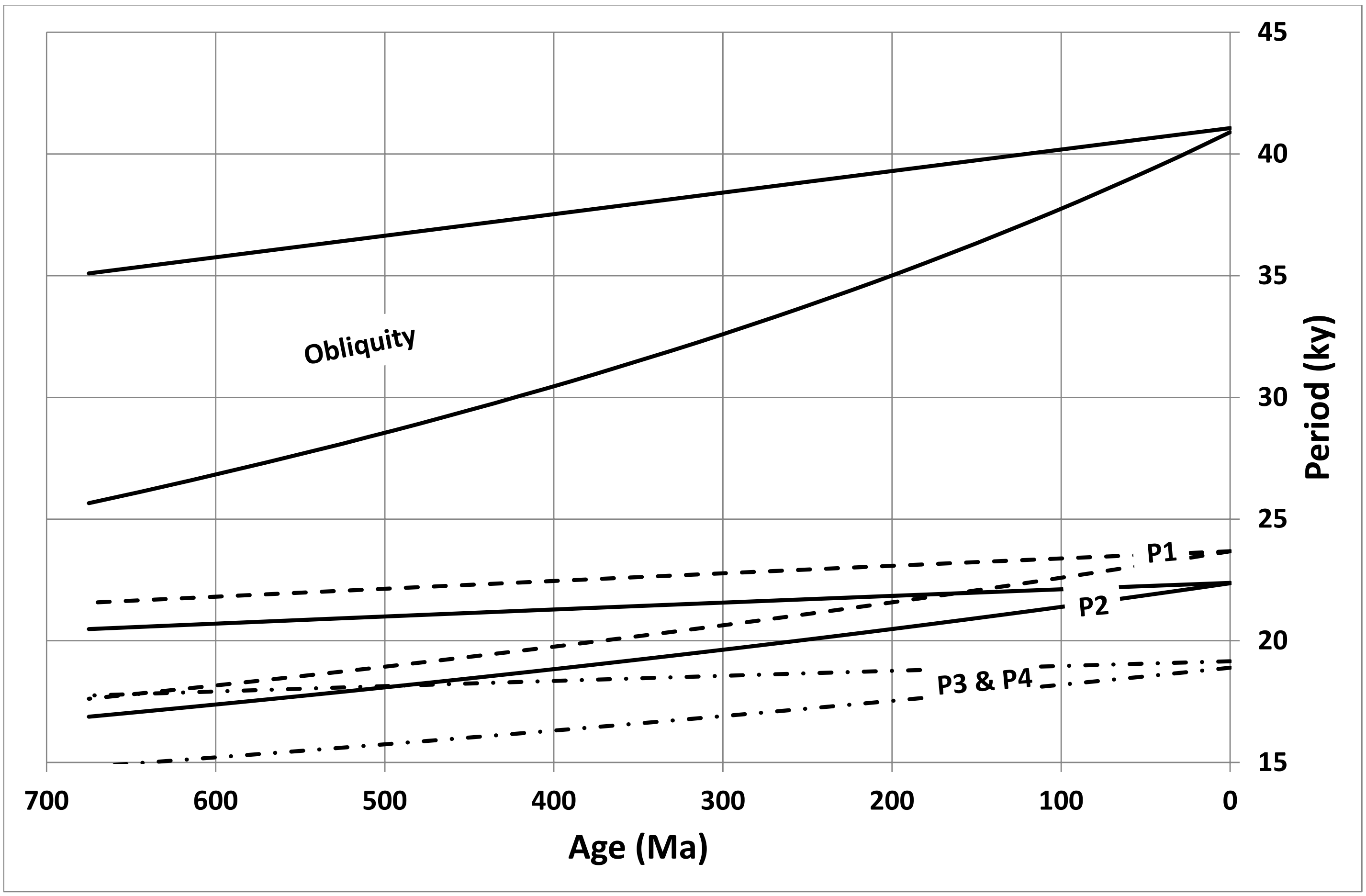

45
40
35
30
25
20
15
Period (ky)
Obliquity
P1
P2
P3 & P4
700
600
500
400
300
200
100
0
Age (Ma)

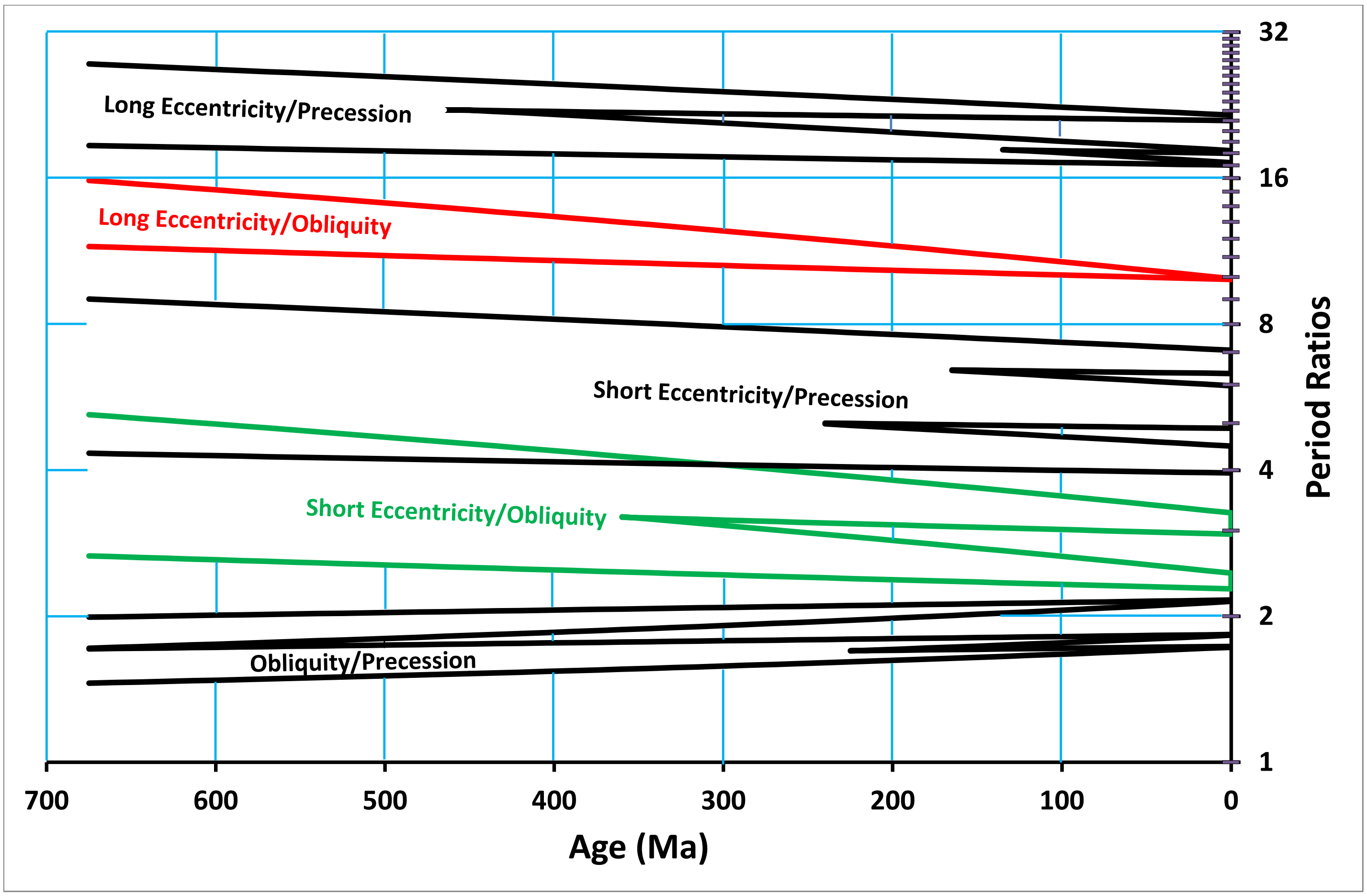

Long Eccentricity/Precession
Long Eccentricity/Obliquity
Short Eccentricity/Precession
Short Eccentricity/Obliquity
Obliquity/Precession
32
16
8
4
2
1
Period Ratios
700
600
500
400
300
200
100
0
Age (Ma)

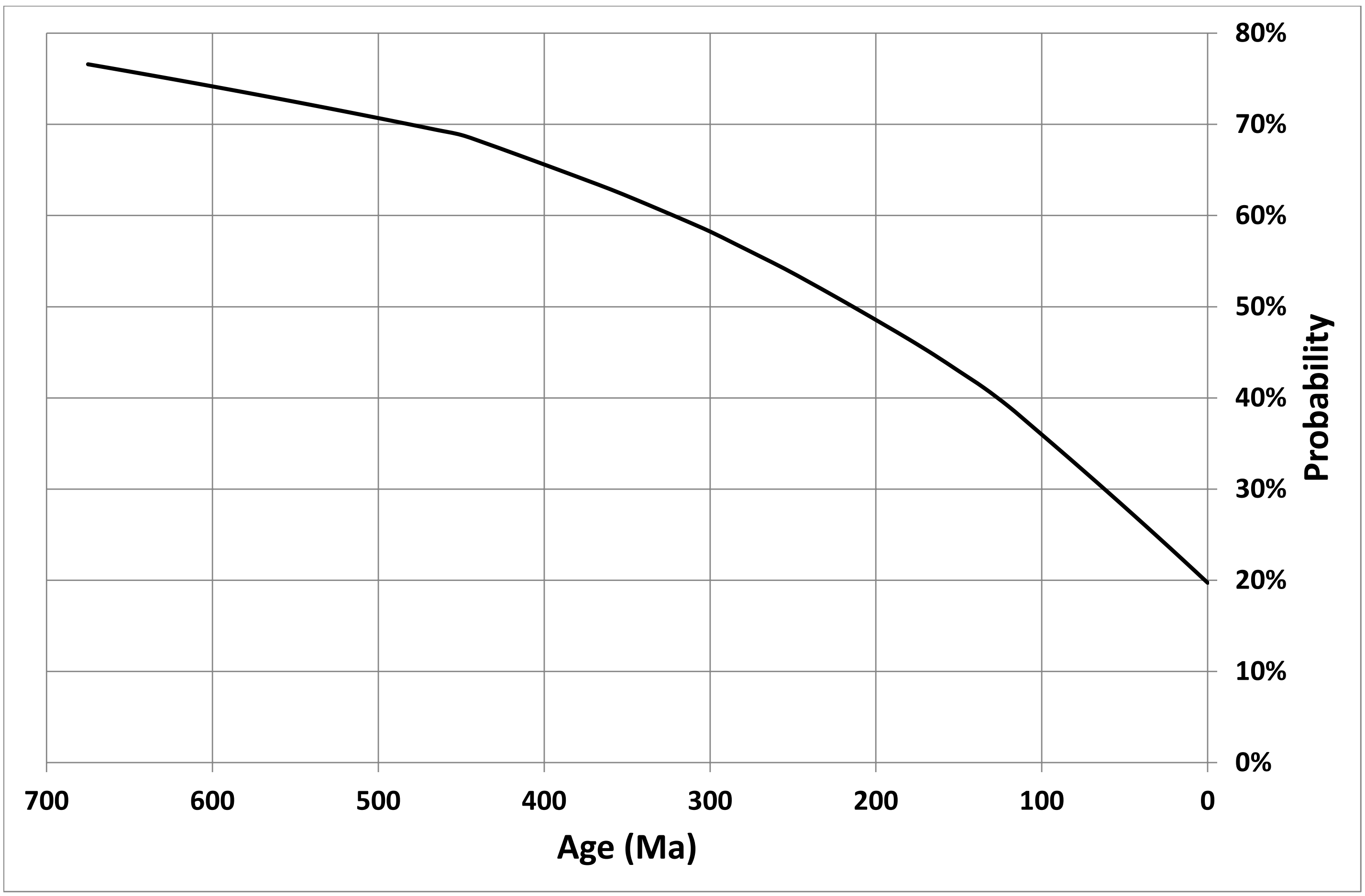
80%
70%
60%
50%
40%
30%
20%
10%
0%
Probability
700
600
500
400
300
200
100
0
Age (Ma)

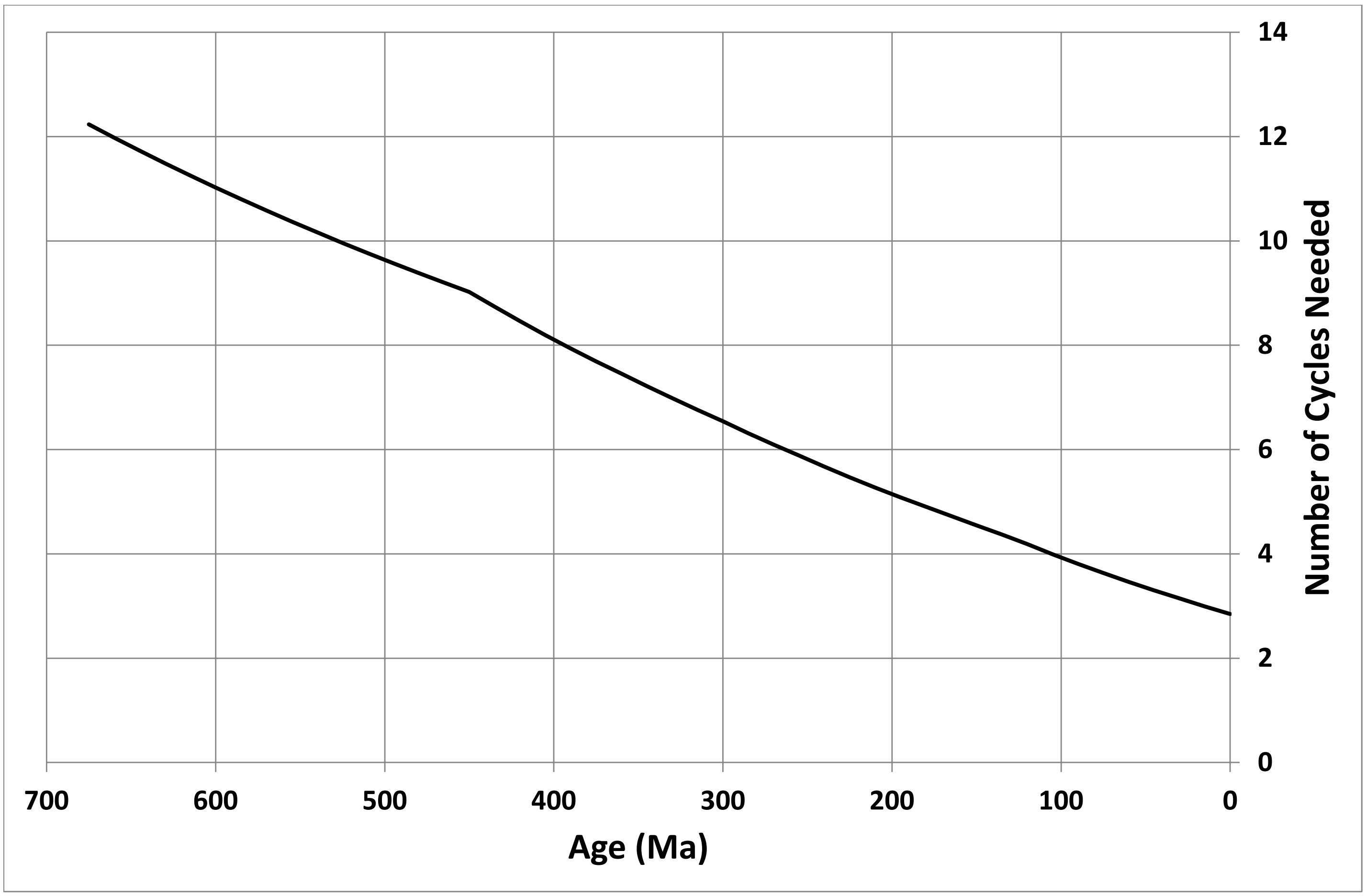
14
12
10
8
6
4
2
0
Number of Cycles Needed
700
600
500
400
300
200
100
0
Age (Ma)

Milankovitch Calculator

Details in: Waltham, D., 2015. Milankovitch Period Uncertainties and Their Impact on Cyclostratigraphy JSR, in review

Age: 300 Ma

Earth-Moon Distance

376.6 ± 4.4 thousand km

Earth Day

22.88 ± 0.61 hours

Earth Axis Mean Obliquity

22.69 ± 0.31 degrees

Earth Axis Precession Period

23.4 ± 1.2 ky

Main Obliquity Period

35.5 ± 2.9 ky

Climatic Precession Periods

21.7 ± 1.1 ky

20.60 ± 0.97 ky

17.66 ± 0.76 ky

17.88 ± 0.77 ky